JACS
JOURNAL OF THE AMERICAN CHEMICAL SOCIETY

ARTICLE

pubs.acs.org/JACS

Catalytic Itinerary in 1,3-1,4-β-Glucanase Unraveled by QM/MM Metadynamics. Charge Is Not Yet Fully Developed at the Oxocarbenium Ion-like Transition State

Xevi Biarnés,[†,§] Albert Ardèvol,[†,‡] Javier Iglesias-Fernández,[†,‡] Antoni Planas,[§] and Carme Rovira*[,†,‡,⊥]

[‡]Institut de Química Teòrica i Computacional de la UB and [†]Computer Simulation and Modeling Laboratory, Parc Científic de Barcelona, Baldiri Reixac 10-12, 08028 Barcelona, Spain

[§]Laboratory of Biochemistry, Institut Químic de Sarrià, Universitat Ramon Llull, Via Augusta, 390, 08017 Barcelona, Spain

[⊥]Institució Catalana de Recerca i Estudis Avançats, Passeig Lluís Companys, 23, 08018 Barcelona, Spain

Supporting Information

ABSTRACT: Retaining glycoside hydrolases (GHs), key enzymes in the metabolism of polysaccharides and glycoconjugates and common biocatalysts used in chemoenzymatic oligosaccharide synthesis, operate via a double-displacement mechanism with the formation of a glycosyl−enzyme intermediate. However, the degree of oxocarbenium ion character of the reaction transition state and the precise conformational itinerary of the substrate during the reaction, pivotal in the design of efficient inhibitors, remain elusive for many GHs. By means of QM/MM metadynamics, we unravel the catalytic itinerary of 1,3-1,4-β-glucanase, one of the most active GHs, belonging to family 16. We show that, in the Michaelis complex, the enzyme environment restricts the conformational motion of the substrate to stabilize a $^{1,4}B/^{1}S_3$ conformation of the saccharide ring at the −1 subsite, confirming that this distortion preactivates the substrate for catalysis. The metadynamics simulation of the enzymatic reaction captures the complete conformational itinerary of the substrate during the glycosylation reaction ($^{1,4}B/^{1}S_3 - {}^{4}E/{}^{4}H_3 - {}^{4}C_1$) and shows that the transition state is not the point of maximum charge development at the anomeric carbon. The overall catalytic mechanism is of dissociative type, and proton transfer to the glycosidic oxygen is a late event, clarifying previous kinetic studies of this enzyme.

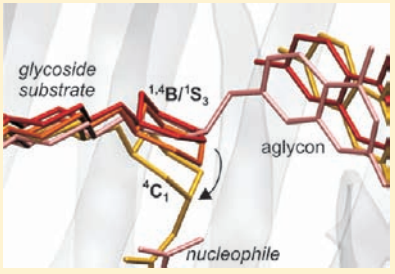

1. INTRODUCTION

Glycoside hydrolases (GHs) are the enzymes responsible for the hydrolysis of glycosidic bonds in carbohydrates. They are the largest group of glycan-degrading enzymes and have important biological functions, such as glycan processing in glycoproteins, remodeling the cell walls, and polysaccharide modification and degradation.[1]

The reaction mechanism of GH, a classic textbook example of an enzymatic reaction, has attracted much interest because genetically inherited disorders of glycoside hydrolysis often occur and because a number of GHs are targets for the design of inhibitors as therapeutic agents against a broad range of diseases (e.g., viral infections[2]). Despite the large number of GH families known (~110, classified according to sequence similarities),[3] they share a common catalytic mechanism: acid/base catalysis with retention or inversion of the anomeric configuration, except for family 4.[4] Inverting GHs operate by a single nucleophilic substitution, while retaining GHs follow a double displacement mechanism via formation of a covalent glycosyl−enzyme intermediate (glycosylation step, Figure 1) followed by hydrolysis of this intermediate (deglycosylation step). Evidence for the formation of a covalent glycosyl−enzyme intermediate is provided by X-ray crystallography on enzyme−inhibitor complexes (see, e.g., ref 5), as well as theoretical calculations using Density Functional Theory (DFT) on lysozyme,[6] β-galactosidase,[7] cellulases,[8] mannanases,[9] and chitinases[10] or semiempirical methods like on *N*-acetylglucosaminidase.[11] Common to both inverting and retaining enzymes is the formation of an oxocarbenium ion-like transition state (TS) during the reaction, as shown by kinetic isotope effect experiments[12] and recent theoretical studies.[6b,7−10,13]

It is now accepted that the substrate undergoes a subtle but critical conformational change upon binding to the GH active site.[14] Specifically, the sugar ring located at the −1 enzyme subsite (hereafter referred as "−1 sugar") distorts away from its $^{4}C_1$ chair conformation in solution toward a distorted (e.g., boat or skew-boat) conformation (Figure 2a).[15] A great effort has been devoted in recent years to decipher the "conformational itinerary" that the substrate follows, not only upon binding to the enzyme but during the reaction as well,[5,14,16] as it has an impact on the design of inhibitors for these enzymes.[16,17] To classify substrate catalytic itineraries, Davies et al.[5,16] used Stoddart's diagram (Figure 2b),[18] which schematically shows all the possible conformers for a single pyranose unit according to their corresponding IUPAC nomenclature.

Received: July 29, 2011
Published: November 01, 2011

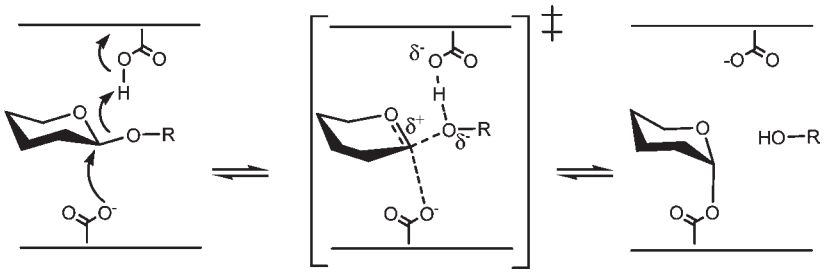

Figure 1. Catalytic mechanism of the glycosylation step in retaining β-glycoside hydrolases (β-GHs). In the case of *Bacillus* 1,3-1,4-β-glucanase, the nucleophile and acid/base residues are Glu105 and Glu109, respectively. The distortion of the sugar ring is not represented.

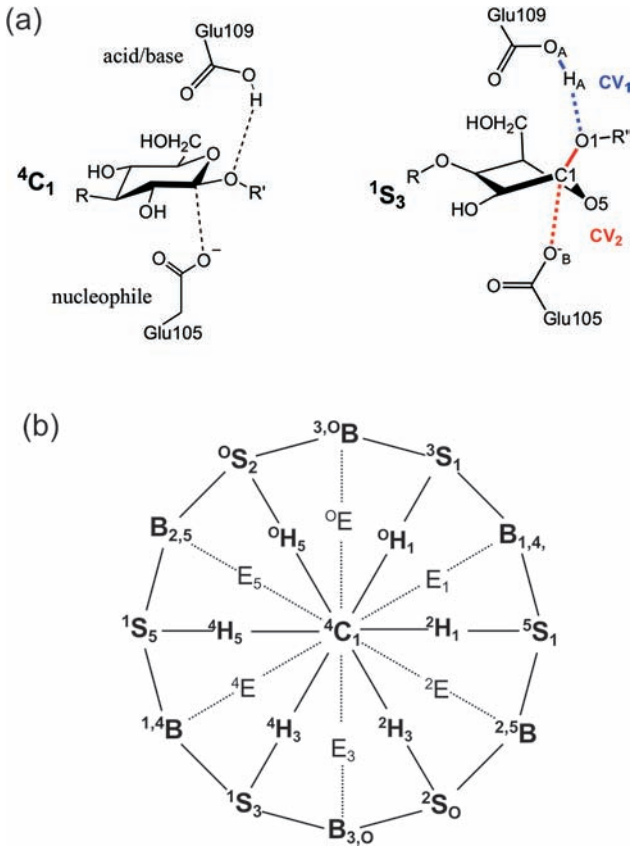

Figure 2. (a) $^4C_1$ chair conformation of the glycosyl unit at the −1 subsite, in comparison with the distorted $^1S_3$ skew-boat conformation. The side chains of the acid/base and nucleophile catalytic residues correspond to those for 1,3-1,4-β-glucanase. Collective variables (CV_1 and CV_2) used to model the hydrolysis of the glycosidic bond are shown (see definition in the text). (b) Stoddart's diagram (centered on the $^4C_1$ conformation).

The structure of the −1 sugar unit in the Michaelis complex, the covalent glycoside intermediate (in the case of retaining GHs), or the product (in the case of inverting GHs) can be associated with one of these conformations, and the conformation at the TS of the reaction can be inferred from the line connecting the two states. Catalytic itineraries have been predicted for only a few GH families,[16] due to the difficulties in trapping the different species along the reaction pathway (not possible using the natural substrate and the wild-type enzyme). In the case of GHs acting on glucose derivatives (glucosidases), two itineraries have been predicted:[16] $^1S_3-^4H_3-^4C_1$ for retaining enzymes and $^2S_O-^{2,5}B-^5S_1$ for inverting enzymes.

Molecular simulation constitutes a useful tool to elucidate the conformation of the substrate in GHs. In a previous study, we showed that the conformational free energy landscape of an isolated β-D-glucopyranose associated with Stoddart's diagram, computed using *ab initio* metadynamics, can be used to predict the conformation of the substrate in the Michaelis complexes of glucosidases.[19] In particular, the conformational map of β-D-glucopyranose shows different energy minima in the region between $^1S_5$ and $^{2,5}B$ (Figure 2b), which is the region where substrate conformations of glucosidases are found. This landscape is expected to change notably once the saccharide ring binds to the active site of a *specific* glucosidase. Understanding these changes and how the substrate changes shape during catalysis is the first step toward rational inhibitor design.

In the framework of our structure/function studies of bacterial 1,3-1,4-β-glucanases, we here investigate the conformational itinerary followed by the glucopyranoside substrate during its catalytic processing in *Bacillus* 1,3-1,4-β-glucanase, one of the most active GHs, belonging to family 16. Experimental information of an enzyme−substrate (E·S) complex structure is currently missing for any member of family 16. By means of quantum mechanics/molecular mechanics (QM/MM) metadynamics, we first analyze the flexibility of the whole substrate bound to the active site before the reaction starts by computing the conformational free energy landscape of the glycosyl unit at the −1 subsite. Next, starting from the computed Michaelis complex structure, we model the rate-limiting step of the catalytic reaction, the formation of the glycosyl−enzyme intermediate. By following the electronic and structural reorganizations at the active site during the reaction pathway, we show that the reaction features a dissociative oxocarbenium-ion-like TS that occurs prior to the maximum development of charge at the anomeric carbon. The reaction conformational itinerary is similar to the one that has been proposed experimentally for retaining glucosidases, although it is not a straight line on Stoddart's diagram as usually assumed but a warped one. Furthermore, it will be shown that there is a relation between the conformations available for the substrate in the Michaelis complex and the conformational itinerary followed by the substrate during catalysis.

2. METHODS

2.1. Hybrid QM/MM Molecular Dynamics Simulations. The initial structure for the simulations was taken from our previous work on the enzyme−substrate complex of *Bacillus* 1,3-1,4-β-glucanase with a 4-methylumbelliferyl (MU) tetrasaccharide (Figure 3),[20] a good substrate extensively used in enzyme kinetics[21] that expands from the −4 to the +1

enzyme subsites (see Figure 3). The glucose unit at the −1 subsite (hereafter referred to as the −1 sugar ring) adopts a distorted conformation that is intermediate between $^{1,4}B$ and $^{1}S_3$ (Figure 3).

QM/MM calculations were performed using the method developed by Laio et al.,[22] which combines Car−Parrinello molecular dynamics (MD),[23] based on DFT, with classical force-field MD. Previous studies showed that this methodology provides an accurate description of energetic, dynamic, and structural features of biological systems, including GHs.[24]

The CPMD program[25] was used for the atoms of the QM region, whereas the Cornell et al. force field,[26] as implemented in the AMBER 7.0 program,[27] and the GLYCAM parameter set[28] were used for the atoms of the MM region. The MU aglycon was parametrized using the antechamber module. The atomic charges of the substrate (ESP) were obtained from a first-principles (Car−Parrinello) calculation of the isolated substrate. The electrostatic interactions between the QM and MM regions were handled via a fully Hamiltonian coupling scheme[22] where the short-range electrostatic interactions between the QM and the MM regions are explicitly taken into account for all MM atoms. An appropriately modified Coulomb potential was used to ensure that no unphysical escape of the electronic density from the QM to the MM region occurs. The electrostatic interactions with the more distant MM atoms were treated via a multipole expansion. All His residues (located in the protein surface) were taken as protonated (i.e., positive charge), and all Asp and Glu residues were taken as deprotonated (i.e., negative charge) except for Glu109 (the acid/base residue) and Asp107, which is hydrogen-bonded to the nucleophile Glu105. Six chlorine atoms were added to achieve neutrality of the protein structure. The system was enveloped in a 52 × 40 × 66 Å box of equilibrated TIP3P water molecules

For the simulations of the substrate conformational map, the QM region was composed of 42 atoms corresponding to the sugar located at the −1 subsite and the MU aglycon, enclosed in an isolated supercell[29] of dimensions 17.5 × 11.1 × 12.2 Å. For the glycosylation reaction simulation, the size of the QM region was enlarged to include the side chains of the catalytic triad residues (Glu105, Asp107, and Glu109), resulting in a total of 65 atoms enclosed in a 18.0 × 14.8 × 16.4 Å isolated supercell. Kohn−Sham orbitals were expanded in a plane-wave basis set with a kinetic energy cutoff of 70 Ry. Norm-conserving Troullier−Martins *ab initio* pseudopotentials[30] were used for all the elements. The PBE functional in the generalized gradient-corrected approximation of DFT was used, consistent with our previous work on 1,3-1,4-β-glucanase.[20] A constant temperature of 300 K was reached by coupling the system to a Nosé−Hoover thermostat[31] at 3500 cm^{-1}. Structural optimizations were done by MD with annealing of the ionic velocities until the maximal component of the nuclear gradient was $<10^{-4}$ au. A time step of 0.12 fs and a fictitious electron mass of 700 au were used in the Car−Parrinello simulations.

2.2. Metadynamics Simulations. The metadynamics approach,[32] in its extended Lagrangian version,[33] was used to enhance the sampling of the phase space and to reconstruct the free energy landscape of the simulated processes with respect to two collective variables (CVs). The general details of this method and its applications to biochemical reactions are available from recent reviews.[34] For the conformational map of the E·S complex, the CVs used are a derivation of the Cremer and Pople puckering coordinates[35] (projection of the Q, θ, and φ polar coordinates onto the equatorial plane, namely q_x and q_y), as used in our previous works on pyranoses.[19,36] The Gaussian height and width were 0.3 kcal·mol^{-1} and 0.15 Å, respectively, and the deposition time was set to 100 MD steps. A total time of 84 ps of simulation (7000 Gaussian potentials) was required to reconstruct the whole energy phase space.

The CVs used for the simulation of the glycosylation reaction were taken as a combination of coordination numbers (CNs) of the covalent bonds being formed/broken (Figure 2b). The CN is given by[33]

$$CN_{ij} = \frac{1-(d_{ij}/d_0)^p}{1-(d_{ij}/d_0)^{p+q}}$$

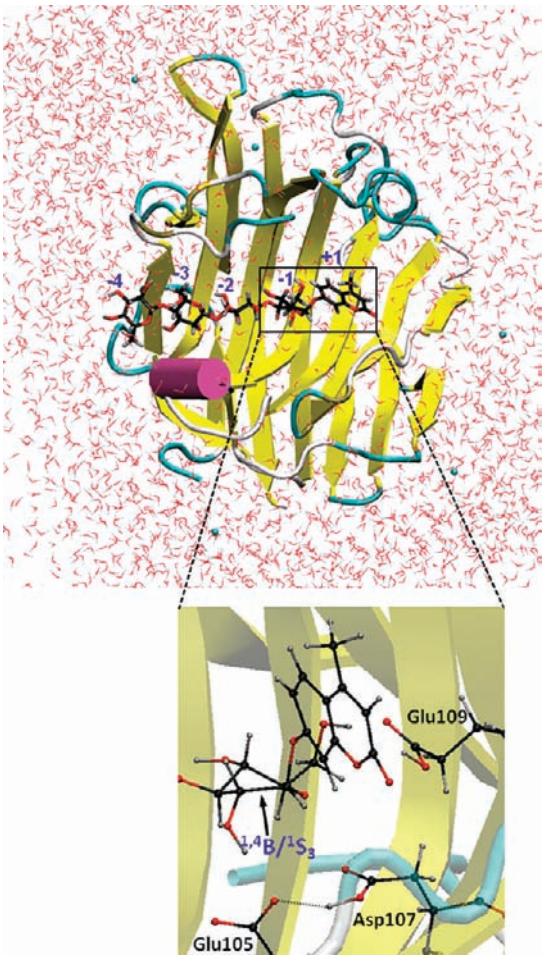

Figure 3. Structure of the Michaelis complex of *Bacillus* 1,3-1,4-β-glucanase with a 4-methylumbelliferyl (MU) tetrasaccharide obtained from QM/MM calculations[20] and used as the initial structure for the metadynamics simulations.

where d_{ij} is the internuclear distance of the atoms involved, d_0 is the threshold bonding distance, and p and q are exponents that determine the steepness of CN_{ij} decay with respect to d_{ij}. CN values range from 0 (not bonded) to 1 (bonded). Since there are up to four bonds being formed/cleaved during the nucleophilic substitution reaction, a bidimensional (two CVs) metadynamics simulation was called for. To describe the nucleophilic attack, we defined CV_1 as the difference in CN between the forming E−S bond (i.e., the bond involving the anomeric carbon and the Glu105 oxygen) and the scissile glycosidic bond (i.e., the bond between the anomeric carbon and the glycosidic oxygen). CV_2 was defined to describe the proton transfer from the Glu109 acid/base catalyst to the incipient alcohol (Figure 2a).

$$CV_1 = CN_{C1\cdots O_B} - CN_{C1\cdots O1}$$

$$CV_2 = CN_{H_A\cdots O1} - CN_{H_A\cdots O_A}$$

The selected metadynamics parameters for each of the CVs were chosen as follows: CV_1, p = 12, q = 14, d_0 = 1.60 Å; CV_2, p = 12, q = 14, d_0 = 1.10 Å). In this way, both CVs take negative values in the E·S Michaelis complex configuration and positive values in the E−S covalent intermediate configuration. Transient configurations halfway between the bonds' formation and cleavage will be reflected with CV values around 0. The selected mass values of the fictitious particles were 10 and 5 amu for CV_1 and CV_2, respectively, and the force constants were set to 1.3 and

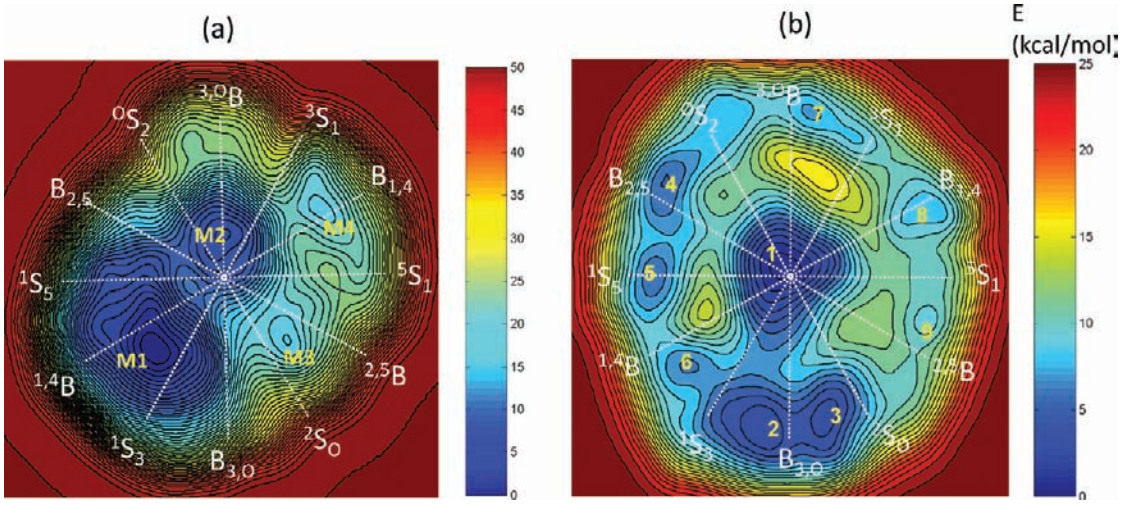

Figure 4. (a) Conformational free energy map of the −1 sugar ring in the E·S complex of 1,3-1,4-β-glucanase obtained from the metadynamics simulation. (b) Conformational free energy map of isolated β-D-glucopyranose,[19] obtained with the same methodology. Contour lines are separated by 1 kcal/mol.

Table 1. Main Distances around the Anomeric Carbon (C1) and Charge of the Anomeric Carbon of the Saccharide Unit at the −1 Subsite Corresponding to the Four Local Minima of the FES (Distances Are in Å and Energies in kcal/mol)

minimum	conformation	C1−O1	C1−O5	$\delta q(C_1)$	E_{rel}
M1	$^{1,4}B/^{1}S_3$	1.51 ± 0.06	1.39 ± 0.04	0.11 ± 0.05	0.0
M2	$^{4}C_1$	1.46 ± 0.04	1.43 ± 0.05	0.06 ± 0.05	6.0
M3	$^{2,5}B/^{2}S_O$	1.45 ± 0.03	1.43 ± 0.04	0.14 ± 0.08	17.5
M4	$B_{1,4}$	1.47 ± 0.05	1.41 ± 0.04	0.06 ± 0.05	18.5

1.4 au, respectively. The height of the Gaussian used was 1.88 kcal·mol^{-1} in the beginning of the simulation and 0.94 kcal·mol^{-1} for a fine determination of the reaction barriers, ensuring sufficient accuracy for reconstructing the free energy surface (FES). The width of the Gaussian terms (0.15 in units of CVs) was selected from the oscillations of the CVs in a free Car−Parrinello QM/MM simulation. A new Gaussian-like potential was added every 200 MD steps. Although values of the height of the Gaussian hills and the deposition time used here (1.88/0.94 kcal mol^{-1} and 24 fs, respectively) are typical for CPMD QM/MM simulations, we should warn that they are still far from the optimum values that were used in the classical formulation of metadynamics (0.025 kcal/mol and 2 ps, respectively). As a consequence, the error on the computed free energies should be considered. It has been shown[37] that the error of the metadynamics depends on the height and width of the Gaussian hills, the deposition time, and the diffusion coefficient of the CVs. Applying the formula derived in ref 37 (the diffusion coefficient was estimated from the time evolution of the mean-square displacement of the CVs) gives an error estimate of 3 kcal/mol. This value is similar to other errors that are expected to affect the results (e.g., the functional employed).

The simulation was stopped after 15.8 ps of simulation, as the system had explored all possible states of interest and a total of 660 Gaussian hills had been deposited. Energy walls at CV_1 = [−0.9:0.9] and CV_2 = [−0.95:0.9] were added to avoid escape of the leaving group during the metadynamics simulation.

The TS was located from commitment analyses.[38] Briefly, small regions along the minimum energy pathway (squares of ±0.05 in terms of CVs) were defined. To locate the TS, we considered four adjacent regions around the point of maximum energy of the reaction pathway. A total 18/34/15/34 structures belong to each region, respectively (see Supporting Information). Commitment analyses[38] were performed on few structures of each region. Only one of them turned out to contain structures committed to either reactants or products. The putative TS was taken as an average of structures in this region. A further commitment analysis on the resulting structure, performed over 100 trajectories, confirmed the goodness of the proposed TS.

3. RESULTS

3.1. Metadynamics Simulation of Ring Puckering in the Michaelis Complex. Metadynamics simulations were performed to explore all possible conformations of the −1 sugar ring in the Michaelis complex and obtain the FES associated with Stoddart's diagram. As CVs, we used a combination of the Cremer and Pople puckering coordinates, as previously done for isolated sugars.[36,19] The reconstructed FES is shown in Figure 4a. Each point in the surface corresponds to a different conformation of the −1 sugar ring. Two main local minima can be distinguished, plus two minor ones. The minima were labeled as M1−M4 according to their relative stability.

The most stable minimum of the FES (M1) turns out to be a distorted conformation half-way between $^{1,4}B$ and $^{1}S_3$. The second minimum in order of stability (M2) corresponds to the $^{4}C_1$ chair, which is 6 kcal/mol higher in energy (see Table 1) than M1 and, therefore, much less populated at room temperature. The transformation barriers from the $^{1}S_3/^{1,4}B$ global minimum to the first local minimum amount to 15 kcal/mol. The remaining two minima (M3 and M4, corresponding to the $^{2}S_O/^{2,5}B$ and $B_{1,4}$ configurations, respectively) are relatively high in energy (>16 kcal/mol), and they can be considered as nonproductive in terms of enzymatic catalysis.

In terms of internal structure and electronic changes, the $^{1}S_3/^{1,4}B$ conformer (M1) shows an increased charge at the anomeric carbon (from 0.06 to 0.11, see Table 1) compared to the undistorted conformer (M2, $^{4}C_1$), a longer glycosidic bond (by 0.05 Å), and a shorter intra-ring C1−O5 distance (by 0.04 Å). These small changes are reminiscent of the oxocarbenium-ion-like TS of the reaction, in which the anomeric carbon acquires positive charge and the glycosidic bond is partially broken. In agreement with our previous MD study of the Michaelis complex of this enzyme,[20] this

indicates that, by favoring small structural and electronic changes around the anomeric carbon, the enzyme preactivates the substrate for the first step of the catalytic reaction. In the next section we will show that these structural and electronic changes keep intensifying along the reaction coordinate.

To analyze the effect of the protein environment in the conformational space available for the −1 sugar unit (a β-D-glucopyranoside), it is interesting to compare the FES of Figure 4a with the one previously obtained for an isolated β-D-glucopyranose,[19] reproduced in Figure 4b. Remarkably, the $^4C_1$ chair is the global minimum of isolated glucopyranose,[19] whereas the sugar ring preferentially adopts a distorted conformation ($^{1,4}B/^1S_3$) in the E·S complex, with the $^4C_1$ chair being a local minimum higher in energy. It is thus clear that the enzyme environment restricts the conformational space available for the glucosyl unit, such that only two main conformations are stabilized ($^4C_1$ and $^{1,4}B/^1S_3$), and *inverts the relative stability of the chair conformer with respect to the most stable distorted structure*.

The limited conformational space available for the −1 sugar ring in the E·S complex, in comparison with an isolated ring, is likely due to two main factors. First are the intermolecular interactions with the protein residues, especially the C2−OH···Glu105$^{(-)}$ hydrogen bond,[20] which restrains the orientation of the hydroxyl substituent at C2. In fact, conformations with an axial C2−OH, such as $^{3,0}B$, are not observed, and all minimum free energy conformations (M1−M4) exhibit an equatorial C2−OH (Table 2). Second, the glycosidic bonds with the −2 and +1 substrate residues (C3−O3 and C1−O1, respectively) restrict the conformational space available for the −1 sugar ring. The C1−O1 bond exhibits either an axial (M1 and M3) or an equatorial orientation (M2 and M4), but the substrate is better adapted to the shape of the binding pocket in the former (the equatorial orientation requires a rotation of the aglycon around the C1−O1 bond).[20] The C3−O3 glycosidic bond, being the link of the −1 ring with the rest of the oligosaccharide, is more rigid than C1−O1. (In fact, the protein residues of the −2, −3, and −4 subsites move little during the metadynamics simulation, in comparison with the residues of the −1 and +1 subsites, Figure S1.) Except for the highest energy conformer (M4), all minima display the most stable equatorial orientation of C3−O3. The axial orientation of C3−O at M4 occurs at the cost of pushing the substrate away from its most stable position by moving up the −1 sugar ring and the aglycon.

Table 2. Orientation of the Ring Exocyclic Groups in the Different Conformations of the Saccharide Ring at the −1 Subsite (*ax* = axial, *eq* = equatorial, *psax* = pseudoaxial)

minimum	C1−O1	C2−O2	C3−O3	C4−O4	C5−O6
M1	*ax*	***eq***	*eq*	*eq*	*eq*
M2	*eq*	***eq***	*eq*	*eq*	*eq*
M3	*ax*	***eq***	*eq*	*ax*	*ax*
M4	*eq*	***eq***	*psax*	*ax*	*ax*

In summary, a combination of steric and intermolecular interactions (hydrogen-bonding) confines the substrate of 1,3-1,4-β-glucanase in two main conformations: a distorted $^{1,4}B/^1S_3$ conformation and the undistorted $^4C_1$ chair conformation, the first one being more favored. Therefore, the simulation of the glycosylation reaction was initiated from the $^{1,4}B/^1S_3$ conformer.

3.2. Metadynamics Simulation of the Glycosylation Reaction. The first step of the enzymatic hydrolysis of the MU tetrasaccharide substrate by *Bacillus* 1,3-1,4-β-glucanase was modeled by QM/MM metadynamics using two CVs (see Methods section). The first variable (CV_1 or *nucleophile attack*) measures the degree of formation of the covalent bond between the substrate and the nucleophile residue. The second variable (CV_2 or *proton transfer*)

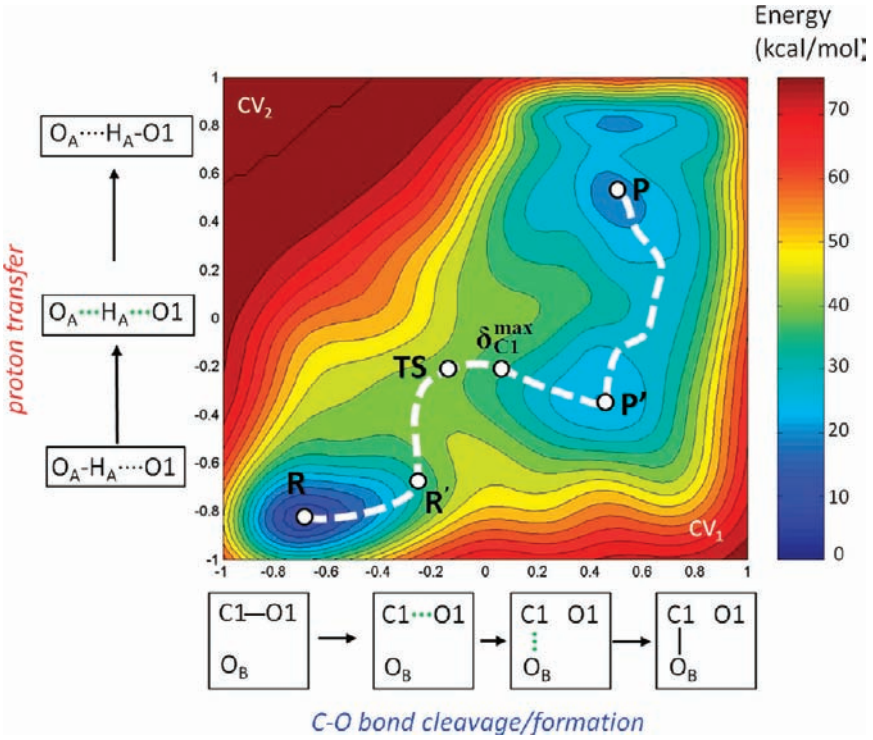

Figure 5. Free energy surface for the formation of the covalent glucosyl−enzyme intermediate in 1,3-1,4-β-glucanase. Contour lines are separated by 4 kcal/mol. The red dots on the axes labels represent the bonds being formed/broken.

dx.doi.org/10.1021/ja207113e |J. Am. Chem. Soc. 2011, 133, 20301–20309

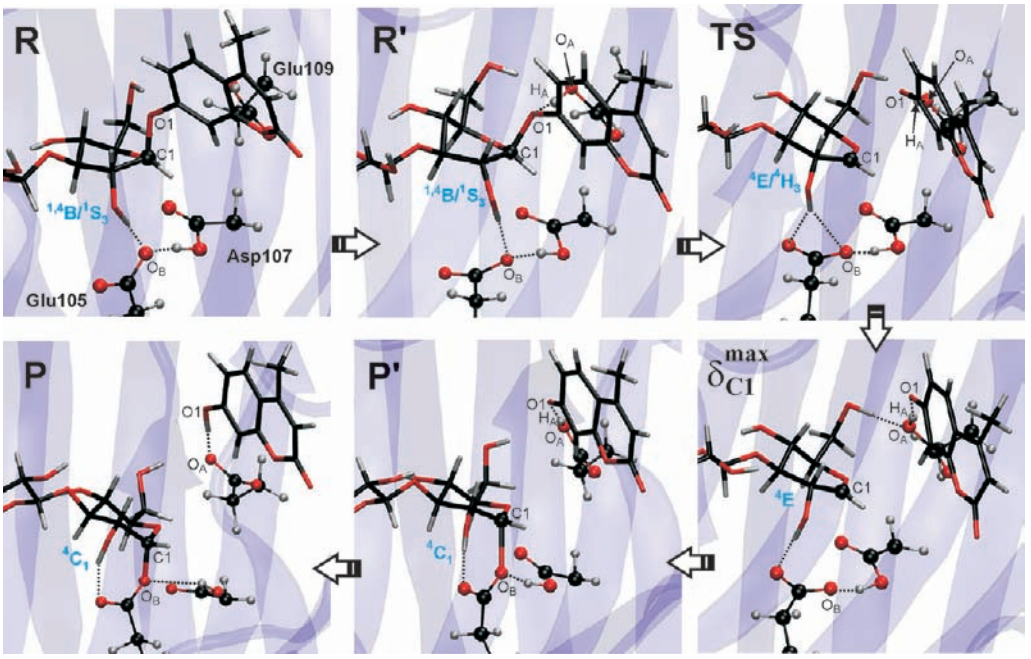

Figure 6. Representative structures along the reaction pathway, corresponding to the stationary points of the reaction free energy surface.

Table 3. Energetic, Structural, and Electronic Parameters of Each Characteristic Point along the Reaction Pathway (See Figure 2a for atom labelling)

	R	R′	TS	δ_{an}^{max}	P′	P
			Distance (Å)			
C1−O1	1.69 ± 0.05	2.38 ± 0.05	3.39 ± 0.31	3.35 ± 0.02	4.83 ± 0.24	5.17 ± 0.87
C1−O_B	3.67 ± 0.21	3.65 ± 0.05	3.61 ± 0.28	2.49 ± 0.02	1.92 ± 0.06	1.98 ± 0.08
O_A−H_A	0.97 ± 0.02	0.99 ± 0.02	1.15 ± 0.02	1.16 ± 0.01	1.06 ± 0.02	1.82 ± 0.07
H_A−O1	2.62 ± 0.19	1.81 ± 0.07	1.32 ± 0.02	1.36 ± 0.01	1.5 ± 0.03	1.00 ± 0.03
C1−O5	1.34 ± 0.01	1.29 ± 0.04	1.28 ± 0.03	1.32 ± 0.01	1.32 ± 0.03	1.30 ± 0.02
			Charge (e)			
C1	0.20 ± 0.04	0.36 ± 0.03	0.49 ± 0.09	0.54 ± 0.01	0.32 ± 0.04	0.27 ± 0.1
O1	−0.01 ± 0.05	−0.02 ± 0.02	−0.19 ± 0.11	−0.20 ± 0.02	−0.27 ± 0.12	−0.18 ± 0.09
O5	−0.29 ± 0.06	−0.28 ± 0.03	−0.25 ± 0.05	−0.26 ± 0.03	−0.28 ± 0.07	−0.33 ± 0.08

quantifies the degree of proton transfer between the acid/base residue and the substrate glycosidic oxygen (Figure 2b).

The variation of the CVs during the metadynamics simulation is provided in the Supporting Information, whereas the FES, reconstructed from the simulation, is shown in Figure 5. Four local minima can be identified. The one on the left-hand side of the diagram corresponds to the reactant state (**R**, the Michaelis complex), whereas the minima on the right-hand side (**P′**, **P**) correspond to different configurations of the products (the covalent glycosyl−enzyme intermediate). The difference between **P′** and **P** lies in the degree of proton transfer (the H_A proton is on the acid/base residue in **P′** but on the aglycon in **P**). The dashed line indicates the minimum free energy path, computed according to the intrinsic reaction coordinate method.[39] The TS was located from commitment analyses[38] (see section 2.2). The resulting TS configuration gave a ratio of 0.49/0.51 over 100 MD trajectories starting with random velocities. The free energy difference between the reactants and the TS (32 kcal·mol^{-1}) is similar to the values previously obtained for GH8 (36 kcal/mol) and GH38 (24 kcal/mol), using a similar methodology.[8,9]

Representative structures of the characteristic points of the FES are shown in Figure 6. Table 3 lists the average distances and atomic charges (using the Restrained Electrostatic Potential approach, RESP) of relevant atoms at the above-defined states **R**, **TS**, **P**, and **P′**. An additional configuration corresponding to the point along the reaction pathway with the maximum charge at the anomeric carbon (state denoted as $\boldsymbol{\delta}_{an}^{max}$) was also analyzed. The properties (structure and electronic charges) of each state were computed from all configurations falling into a small region (±0.05 in terms of the CVs) around the corresponding point of the FES. Complementing this information, Figure 7 shows the evolution of the main distances involving the anomeric carbon (C1′−O1, C1−O_B, H_A−O1, and O_A−H_A), as well as atomic charges of C1, O1, and O5 along the reaction pathway. At the

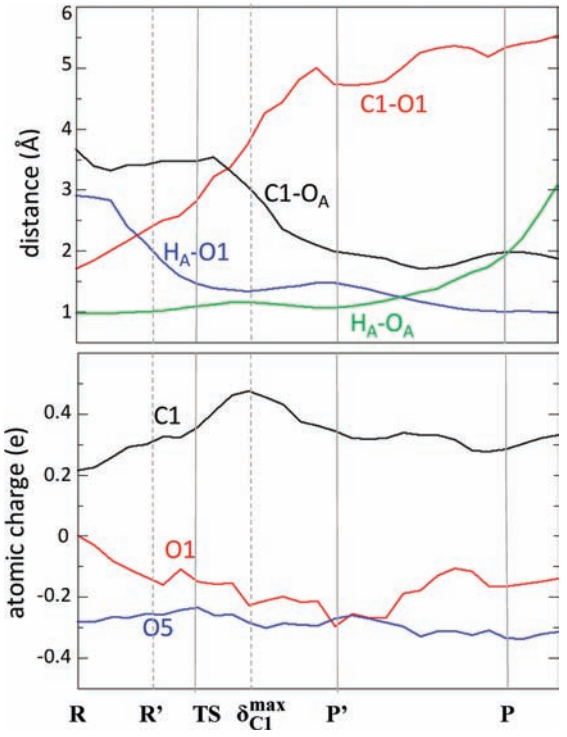

Figure 7. Variation of the relevant distances (C1−O1, C1−O_A, H_A−O1, and H_A−O_A) and charges (C1, O1, and O5) along the reaction pathway. A running average over four data values is taken.

reactant state (**R**), the nucleophile residue (Glu105) is still far from the C1 atom (3.67 Å, Table 3), and it forms a hydrogen bond with Asp107 ($O_B\cdots HO_{Asp107}$, see Figure 6). The acid/base residue (Glu109) does not form a hydrogen bond with the glycosidic oxygen ($H_A\cdots O1$ = 2.62 Å) yet, but points toward the center of the aromatic ring of the MU aglycon.

Reaction Pathway. The reaction begins with the elongation of the glycosidic bond and the simultaneous formation of the hydrogen bond between Glu109 and the glycosidic oxygen. Glu109 changes hydrogen bond partner from the π-system of the MU aglycon to the glycosydic oxygen (the $H_A\cdots O1$ distance decreases from 2.62 to 1.81 Å, in which negative charge is being developed). This places the acidic hydrogen atom at the proper position to assist the departure of the leaving group. This situation is represented by the **R′** state on the reaction pathway of Figure 5. The need for assistance by the acid/base residue is not surprising since the MU aglycon is just a moderately good leaving group ($pK_a \approx 7$). The system reaches the reaction TS when the glycosidic bond increases to 3.39 Å (Table 3). In contrast, the nucleophile (Glu105) practically does not move (C1−O_B slightly decreases from 3.65 to 3.61 Å at the TS), which is indicative of a dissociative type of TS. We thus conclude that the glycosylation reaction in 1,3-1,4-β-glucanase follows a $D_N{}^*A_N$ mechanism, where the glycosidic bond breaks before nucleophilic attack occurs.

The reaction TS is characterized by a short intra-ring C1−O5 bond (it shrinks from 1.34 to 1.28 Å from **R** to **TS**), indicating the formation of a partial double bond, and an increased charge qon the anomeric carbon (from 0.20 to 0.49 e). The in-plane configuration of the C2, C1, O5, and H1 atoms at the TS is consistent with sp^2 hybridization of C1 (see Figure 6). All these changes reveal the presence of a species with oxocarbenium-ion-like

Table 4. Values of the Puckering Coordinates of the Substrate for the Characteristic Points of the FES, as Well as the Point Corresponding to the Configuration with Maximum Anomeric Charge (δ_{an}^{max})[a]

	Q	θ	φ
R	0.59	70.3	238.3
TS	0.55	59.0	218.1
δ_{an}^{max}	0.54	51.9	233.1
P′	0.52	45.2	235.7
P	0.52	25.5	253.7

[a] The puckering coordinates of all states along the complete reaction pathway are given in the Supporting Information.

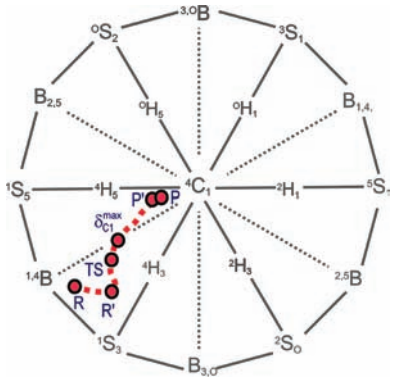

Figure 8. Reaction path of the glycosylation reaction projected onto Stoddart's diagram (i.e., conformational itinerary of the glycosyl unit of the −1 subsite), obtained from the puckering coordinates of all configurations along the predicted reaction pathway. A running average over four data values is taken.

character. Interestingly, the maximum charge of the anomeric carbon (δ_{an}^{max} in Figures 5 and 7) does not occur at the TS but later on the reaction pathway. At this point, both the nucleophile and the leaving group are well separated from the C1 atom. The charge on the anomeric carbon (+0.54) is higher than the TS charge (+0.49e), and the C1−O5 bond is about the same (1.28−1.29 Å). The calculations thus reveal that the glycosylation reaction features an early TS with respect to charge development on the anomeric carbon.

From the TS and going downhill to the products, the C1−O1 keeps increasing (up to 4.83 Å) and the bond between the enzyme nucleophile and the −1 glycosyl unit forms (C1−O_B decreases to 1.92 Å), completing the glycosylation reaction. The acid/base residue is still protonated at **P′** (O_A−H_A = 1.06 Å), and the hydrogen bond with the leaving group persists. The transfer of the proton from the acid/base residue to the aglycon occurs from **P′** to **P** (O_A−H_A increases from 1.06 to 1.83 Å, while O1−H_A decreases to 1.01 Å, see Table 3) and involves a low activation energy (5 kcal/mol).

Substrate Conformational Itinerary. To analyze in detail the conformations of the −1 glycosyl unit of the substrate during the reaction, we extracted the puckering coordinates of all configurations along the predicted reaction pathway (Figure 5 and Table 4) and projected them over Stoddart's diagram (Figure 8). The computed conformational itinerary is similar to the ideal itinerary predicted from the available Michaelis complex structures and glycosyl−enzyme intermediates of glucosidases

($^1S_3 \rightarrow {}^4H_3 \rightarrow {}^4C_1$). However, the stationary points of the reaction FES (**R**, **TS**, **P′**, and **P**) do not correspond to canonical conformations in Stoddart's diagram but intermediate ones. In particular, the reactants state is displaced toward $^{1,4}B$, and the TS moves toward ^4E, such that the precise itinerary is $^{1,4}B/^1S_3 \rightarrow {}^4E/^4H_3 \rightarrow {}^4C_1$. Overall, the reaction itinerary is not a radial straight line on Stoddart's diagram, as usually assumed, but a warped one. Obviously, other glucosidases might exhibit a different itinerary on the southwest quadrant of Stoddart's diagram (in fact, Michaelis complex glucosidase structures are found on a wide region from $^1S_5$ to $^1S_3$),[19] and we might speculate that they will also exhibit similar warped itineraries, with $^1S_3 \rightarrow {}^4H_3 \rightarrow {}^4C_1$ best viewed as a *representative itinerary*.

It is to be noted that the computed substrate conformational itinerary during the reaction is not far from the minimum free energy pathway that connects the two main minima of the FES of the Michaelis complex ($^{1,4}B/^1S_3 \rightarrow E_5/^4H_5 \rightarrow {}^4C_1$, Figure 4a).[40] This indicates that the enzyme active site is engineered to accommodate only a limited number of substrate conformers either before or during the catalytic reaction. Consequently, the conformational free energy diagram of the −1 substrate ring in the enzyme can be used to propose the conformational itinerary of this ring during the hydrolysis reaction in glycosyl hydrolases.

4. DISCUSSION

Following our previous studies on pyranoside ring conformational itineraries,[36,19] we investigated the effect of the enzyme environment on the conformations accessible to a glucopyranoside ring and its possible implications on enzyme catalysis. The target of our study, 1,3-1,4-β-glucanase, is one of the more active GHs, for which structural information about the Michaelis complex is still unknown. *Ab initio* (Car−Parrinello) MD simulations, within the QM/MM approach, were applied to the complex of 1,3-1,4-β-glucanase with a MU tetrasaccharide substrate. Both the free energy conformational map of the substrate in the Michaelis complex state and the FES of the rate-limiting step of the glycolytic reaction have been computed by means of the metadynamics method.

Our results for the Michaelis complex indicate that the substrate is tightly confined in the enzyme cavity. The flexibility of the substrate ring located at the −1 subsite is notably reduced in comparison to that of a free glucopyranoside unit (Figure 4). This conformational confinement imposes severe restrictions on the itinerary that the substrate can follow during the catalytic reaction. Indeed, the $^{1,4}B/^1S_3$ (Michaelis complex) $\rightarrow {}^4E/^4H_3$ (TS) $\rightarrow {}^4C_1$ (product) itinerary, predicted from the conformational free energy map (Figure 4a), resembles the substrate itinerary obtained when simulating the first step of the catalytic reaction (Figure 8). Therefore, evaluation of the conformational free energy map of the −1 sugar ring provides a first approximation to the preferred catalytic itinerary.

The simulation of the glycosylation reaction shows that the TS has a substantial oxocarbenium ion character. The activation energy is invested predominantly in the cleavage of the glycosidic bond, with assistance from the acid/base residue (Glu109) via the formation of a hydrogen bond with the glycosidic oxygen. The nucleophile residue (Glu105) does not participate in the first stage of the reaction, as the C_1-O_B distance remains invariable from the reactants to the TS. Therefore, the driving force of the reaction is the formation of a key hydrogen bond between the acid/base residue and the glycosidic oxygen. Once the glycosydic bond breaks, formation of the glycosyl−enzyme intermediate is a low energy barrier process. Thus, the overall reaction is of dissociative type, in which the glycosidic bond cleavage precedes the formation of the glycosyl−enzyme bond.

Analysis of the evolution of the anomeric charge during the reaction pathway reveals an interesting feature: the maximum oxocarbenium ion character of the −1 sugar ring ($\boldsymbol{\delta}_{an}^{max}$, see Figures 5 and 7) does not coincide with the TS but takes place afterward, showing that the TS of the glycosylation reaction corresponds to an early TS with respect to charge development on the anomeric carbon. In fact, the maximum sp^2 character (measured as the degree of planarity of the local structure around C1) of the anomeric carbon occurs between the TS and $\boldsymbol{\delta}_{an}^{max}$. The conformation of the sugar ring at $\boldsymbol{\delta}_{an}^{max}$ is similar to that of the TS, but the structure of the active site is slightly different (the nucleophile is 1.2 Å closer to the anomeric carbon). As a result, the enzyme stabilizes the charge development at the anomeric carbon, lowering the energy of the corresponding state and displacing the TS earlier in the pathway.

Another interesting feature of the FES is that there is an additional local minimum (**P′**) between the TS and the final product state **P**. **P′** represents an intermediate state in which the leaving group is not yet protonated, although it is hydrogen-bonded to the acid/base residue. The presence of this intermediate can be interpreted in terms of the chemical properties of the leaving group. Since the MU aglycon is a relatively good leaving group ($pK_a \approx 7$), the reaction can take place without its protonation (from **R** to **P′**), even though protonation is required to complete the reaction (from **P′** to **P**). In the case of a poorer leaving group (e.g., a sugar alcohol), one would expect **P′** to vanish. This was the case, for instance, for the cleavage of two mannosyl residues by Golgi α-mannosidase II (GMII), a family 38 retaining GH.[9] In contrast, a good leaving group such as *p*-dinitrophenyl would stabilize **P′** at the expense of **P**. Therefore, the final shape of the FES in the products region reflects the nature of the leaving group.

Interestingly, the Hammet−Brønsted plot of the 1,3-1,4-β-glucanase-catalyzed hydrolysis of a family of aryl glycoside substrates[41] (i.e., $\log k_{cat}$ vs pK_a of the leaving group) exhibits a dual behavior: high slope ($\beta = -0.9$) for good leaving groups ($pK_a < 7$) and little slope ($\beta \approx 0$) for bad ones ($pK_a > 7$). The experimental results were interpreted as a change in TS structure depending on the aglycon.[41] In the light of our calculations, this can be re-interpreted as a change in the sequence of glycosidic bond cleavage vs glycosidic oxygen protonation during the reaction mechanism. Good leaving groups lead to cleavage without protonation and bad leaving groups require protonation prior to bond cleavage. The MU aglycon falls at the intersection between both groups of substrates; therefore, it was not possible to discern whether it exhibits one behavior or the other from an experimental point of view. Our calculations clearly show that protonation occurs after the formation of the covalent glycosyl−enzyme bond. Therefore, the MU aglycon can be considered as belonging to the first group of substrates, i.e., those exhibiting a high dependence of k_{cat} on the pK_a. Like the MU tetrasaccharide used here, these substrates are characterized by a TS with extensive C1−O1 bond cleavage (dissociative) and little protonation on O1, with the concomitant negative charge accumulation on the aglycon oxygen.

■ ASSOCIATED CONTENT

Supporting Information. Further simulation details and analysis of the metadynamics trajectories; ring puckering and

protein coordinates along the reaction pathway. This material is available free of charge via the Internet at http://pubs.acs.org.

AUTHOR INFORMATION

Corresponding Author
crovira@pcb.ub.es

ACKNOWLEDGMENT

We thank Alessandro Laio for valuable support concerning the metadynamics simulations. We acknowledge the Spanish Ministry of Science and Innovation (MICINN) (grant FIS2008-03845 and BFU2010-22209-C02-02) and the Generalitat de Catalunya (GENCAT) (grants 2009SGR-1309 and 2009SGR-82) for its financial assistance. A.A. and X.B. acknowledge a FPU fellowship from MCINN and a Beatriu de Pinós postdoctoral fellowship from GENCAT, respectively. We acknowledge the computer support, technical expertise, and assistance provided by the Barcelona Supercomputing Center-Centro Nacional de Supercomputación.

REFERENCES

(1) Gamblin, D. P.; Scanlan, E. M.; Davis, B. G. *Chem. Rev.* **2009**, *109*, 131–163.
(2) (a) Davies, G.; Henrissat, B. *Structure* **1995**, *3*, 853–859. (b) Alper, J. *Science* **2001**, *291*, 2339.
(3) Cantarel, B. L.; Coutinho, P. M.; Rancurel, C.; Bernard, T.; Lombard, V.; Henrissat, B. *Nucleic Acids Res.* **2009**, *37*, D233–238.
(4) (a) Yip, V. L.; Varrot, A.; Davies, G. J.; Rajan, S. S.; Yang, X.; Thompson, J.; Anderson, W. F.; Withers, S. G. *J. Am. Chem. Soc.* **2004**, *126*, 8354–8355. (b) Vasella, A.; Davies, G. J.; Bohm, M. *Curr. Opin. Chem. Biol.* **2002**, *6*, 619–629.
(5) Davies, G. J.; Ducros, V. M.; Varrot, A.; Zechel, D. L. *Biochem. Soc. Trans.* **2003**, *31*, 523–527.
(6) (a) Bottoni, A.; Miscione, G. P.; De Vivo, M. *Proteins* **2005**, *59*, 118–130. (b) Bowman, A. L.; Grant, I. M.; Mulholland, A. J. *Chem. Commun.* **2008**, 4425–4427.
(7) Bras, N. F.; Moura-Tamames, S. A.; Fernandes, P. A.; Ramos, M. J. *J. Comput. Chem.* **2008**, *29*, 2565–2574.
(8) Petersen, L.; Ardevol, A.; Rovira, C.; Reilly, P. J. *J. Phys. Chem. B* **2009**, *113*, 7331–7339.
(9) Petersen, L.; Ardevol, A.; Rovira, C.; Reilly, P. J. *J. Am. Chem. Soc.* **2010**, *132*, 8291–8300.
(10) Jitonnom, J.; Lee, V. S.; Nimmanpipug, P.; Rowlands, H. A.; Mulholland, A. J. *Biochemistry* **2011**, *50*, 4697–4711.
(11) Lameira, J.; Alves, C. N.; Tunon, I.; Marti, S.; Moliner, V. *J. Phys. Chem. B* **2011**, *115*, 6764–6775.
(12) Selwood, T.; Sinnott, M. L. *Biochem. J.* **1990**, *268*, 317–323.
(13) Barker, I. J.; Petersen, L.; Reilly, P. J. *J. Phys. Chem. B* **2010**, *114*, 15389–15393.
(14) Davies, G. J.; Planas, A.; Rovira, C. *Acc. Chem. Res.* **2011**, DOI 10.1021/ar2001765.
(15) (a) Sulzenbacher, G.; Driguez, H.; Henrissat, B.; Schulein, M.; Davies, G. J. *Biochemistry* **1996**, *35*, 15280–15287. (b) Tews, I.; Perrakis, A.; Oppenheim, A.; Dauter, Z.; Wilson, K. S.; Vorgias, C. E. *Nat. Struct. Biol.* **1996**, *3*, 638–648. (c) Garcia-Herrero, A.; Montero, E.; Munoz, J. L.; Espinosa, J. F.; Vian, A.; Garcia, J. L.; Asensio, J. L.; Canada, F. J.; Jimenez-Barbero, J. *J. Am. Chem. Soc.* **2002**, *124*, 4804–4810.
(16) Vocadlo, D. J.; Davies, G. J. *Curr. Opin. Chem. Biol.* **2008**, *12*, 539–555.
(17) Marcelo, F.; He, Y.; Yuzwa, S. A.; Nieto, L.; Jimenez-Barbero, J.; Sollogoub, M.; Vocadlo, D. J.; Davies, G. D.; Bleriot, Y. *J. Am. Chem. Soc.* **2009**, *131*, 5390–5392.
(18) *Stereochemistry of carbohydrates*; Stoddart, J. F., Ed.; John Wiley & Sons Inc.: Toronto, 1971.
(19) Biarnés, X.; Ardevol, A.; Planas, A.; Rovira, C.; Laio, A.; Parrinello, M. *J. Am. Chem. Soc.* **2007**, *129*, 10686–10693.
(20) Biarnes, X.; Nieto, J.; Planas, A.; Rovira, C. *J. Biol. Chem.* **2006**, *281*, 1432–1441.
(21) (a) Piotukh, K.; Serra, V.; Borriss, R.; Planas, A. *Biochemistry* **1999**, *38*, 16092–16104. (b) Faijes, M.; Perez, X.; Perez, O.; Planas, A. *Biochemistry* **2003**, *42*, 13304–13318.
(22) Laio, A.; VandeVondele, J.; Rothlisberger, U. *J. Chem. Phys.* **2002**, *116*, 6941–6947.
(23) Car, R.; Parrinello, M. *Phys. Rev. Lett.* **1985**, *55*, 2471–2474.
(24) (a) Carloni, P.; Rothlisberger, U.; Parrinello, M. *Acc. Chem. Res.* **2002**, *35*, 455–464. (b) Dal Peraro, M.; Ruggerone, P.; Raugei, S.; Gervasio, F. L.; Carloni, P. *Curr. Opin. Struct. Biol.* **2007**, *17*, 149–156.
(25) *CPMD* program, IBM Corp., 1990−2003; MPI für Festkörperforschung, Stuttgart, 1997−2001; http://www.cpmd.org.
(26) Cornell, W. D.; Cieplak, P.; Bayly, C. I.; Gould, I. R.; Merz, K. M.; Ferguson, D. M.; Spellmeyer, D. C.; Fox, T.; Caldwell, J. W.; Kollman, P. A. *J. Am. Chem. Soc.* **1995**, *117*, 5179–5197.
(27) Pearlman, D. A.; Case, D. A.; Caldwell, J. W.; Ross, W. S.; Cheatham, T. E.; Debolt, S.; Ferguson, D.; Seibel, G.; Kollman, P. *Comput. Phys. Commun.* **1995**, *91*, 1–41.
(28) Woods, R. J.; Dwek, R. A.; Edge, C. J.; Fraserreid, B. *J. Phys. Chem.* **1995**, *99*, 3832–3846.
(29) Martyna, G. J.; Tuckerman, M. E. *J. Chem. Phys.* **1999**, *110*, 2810–2821.
(30) Troullier, N.; Martins, J. L. *Phys. Rev. B: Condens. Matter.* **1991**, *43*, 1993–2006.
(31) Nosé, S. *J .Chem. Phys.* **1984**, *81*, 511–519.
(32) Laio, A.; Parrinello, M. *Proc. Natl. Acad. Sci. U.S.A.* **2002**, *99*, 12562–12566.
(33) Iannuzzi, M.; Laio, A.; Parrinello, M. *Phys. Rev. Lett.* **2003**, *90*, 238302.
(34) (a) Leone, V.; Marinelli, F.; Carloni, P.; Parrinello, M. *Curr. Opin. Struct. Biol.* **2010**, *20*, 148–154. (b) Barducci, A.; Bonomi, M.; Parrinello, M. *WIREs Comput. Mol. Sci.* **2011**, *1*, 826–843. (c) Biarnes, X.; Bongarzone, S.; Vargiu, A. V.; Carloni, P.; Ruggerone, P. *J. Comput.-Aided Mol. Des.* **2011**, *25*, 395–402.
(35) Cremer, D.; Pople, J. A. *J. Am. Chem. Soc.* **1975**, *97*, 1354–1358.
(36) Ardèvol, A.; Biarnes, X.; Planas, A.; Rovira, C. *J. Am. Chem. Soc.* **2010**, *132*, 16058–16065.
(37) Laio, A.; Rodriguez-Fortea, A.; Gervasio, F. L.; Ceccarelli, M.; Parrinello, M. *J. Phys. Chem. B* **2005**, *109*, 6714–6721.
(38) (a) Dellago, C.; Bolhuis, P. G.; Csajka, F.; Chandler, D. *J. Chem. Phys.* **1998**, *108*, 1964–1977. (b) Peters, B. *Chem. Phys. Lett.* **2000**, *494*, 100–103.
(39) Fukui, K. *Acc. Chem. Res.* **1981**, *14*, 363–368.
(40) Note that the puckering of the sugar ring is not a proper reaction coordinate for the catalytic reaction. Therefore, it is not expected that all characteristic points of the reaction FES appear in different regions of the FES of the ring puckering in the Michaelis complex (e.g., the ring adopts a chair conformation in both **P** and **P**′).
(41) Planas, A.; Abel, M.; Millet, O.; Palasi, J.; Pallares, C.; Viladot, J. L. *Carbohydr. Res.* **1998**, *310*, 53–64.